analytical chemistry

Article

Cite This: *Anal. Chem.* 2019, 91, 2861−2868

pubs.acs.org/ac

Ultrasensitive Photoelectrochemical Detection of Multiple Metal Ions Based on Wavelength-Resolved Dual-Signal Output Triggered by Click Reaction

Han-Mei Deng, Liao-Jing Huang, Ya-Qin Chai, Ruo Yuan,* and Ya-Li Yuan*

Key Laboratory of Luminescent and Real-Time Analytical Chemistry (Southwest University), Ministry of Education, College of Chemistry and Chemical Engineering, Southwest University, Chongqing 400715, PR China

Supporting Information

ABSTRACT: In this work, a click reaction-triggered wavelength-resolved dual-signal output photoelectrochemical (PEC) biosensor with DNAzymes-assisted cleavage recycling amplification was proposed for sensitive triplex metal ions assay. Substantial DNA fragments azido-S_1 and azido-S_2, derived from the Pb^{2+} (target 1) and Mg^{2+} (target 2) dependent cleavage cycle of DNAzymes, respectively, were grafted efficiently on the same alkynyl-DNA (capture DNA) modified electrode via the Cu^{2+} (target 3) and ascorbic acid (AA) cocatalyzed click reaction, which thus could be subsequently used for immobilization of two different photoactive nanomaterials labeled with single DNA to generate distinguishing dual-signal output for simultaneously sensitive detection of Pb^{2+} and Mg^{2+}. Furthermore, the control variable method was used for detecting Cu^{2+} by altering the concentration of Cu^{2+} in the click reaction. Owing to the usage of the click reaction and target-converted signal amplifying strategy, the utilization rate of cycle output DNAs was largely increased, significantly improving the detection sensitivity of the proposed approach. As a result, low detection limits down to picomolar were acquired for the detection of Pb^{2+}, Mg^{2+}, and Cu^{2+}, providing a versatile, efficient, and sensitive PEC method for multiple assays of various targets such as metal ions, small molecules, and tumor markers.

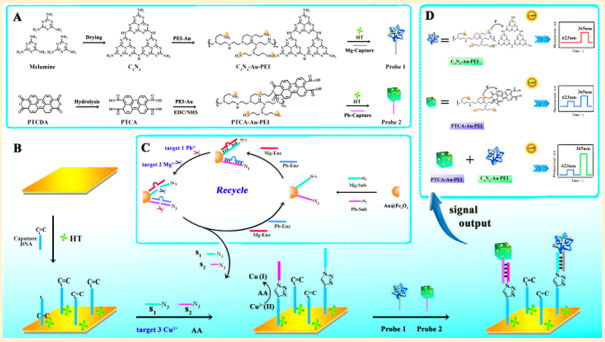

The photoelectrochemical (PEC) biosensor, as a newly emerged analytical device that combines electrochemistry with photochemistry, has been developed rapidly in recent years.[1−5] Apart from the advantages of simple, low cost, and easy operation, the PEC biosensor also exhibits the merits of high sensitivity and low background noise due to the total separation of the excitation source of light and the readout signal of current.[6−9] More importantly, the generation of photocurrent in PEC analysis heavily depends on the photoactive material,[10−16] excitation wavelength,[17,18] and applied potential[19] in the detection process, which holds significant promise for the multiplex assay with advantages of low sample consumption, higher throughput, higher detection efficiency, simpler analytical process, and lower analytical cost. Unfortunately, most reported PEC biosensors mainly focus on the development of sensing platforms for individual analytes,[20−23] and there are only a few works established in PEC biosensors for multiple targets owing to the challenge in distinguishing photocurrent signals from diverse targets. Recently, Hu's group constructed a PEC electrode array to, respectively, acquire target related photocurrent signals for successfully achieving multiplex detection with the use of light addressable technology.[24,25] However, this approach suffered from the drawback of limited sensitivity due to the incomplete coverage of the light source on different minute areas. To circumvent this issue, Dai and Chen's group co-immobilized two capture probes on a single electrode for, respectively, fabricating the applied potential[26] and electron donating[27] resolved multiplex PEC biosensors with improved sensitivity. Nevertheless, to meet the increasing demand of trace multiplex detection, the sensitivity of these multiplex PEC biosensors still needed to be further improved without effective signal amplifying strategies. Accordingly, by integrating the target-induced recycling amplification with wavelength-resolved technology, our group constructed a sensitive PEC biosensor for simultaneous dual components assay.[28] However, the cycle output DNA with poor utilization rate limited the further improvement of detection sensitivity. Therefore, it is necessary and urgent to explore new strategies to significantly increase the utilization rate of output DNAs for constructing a highly sensitive multiple PEC assay with the coupling of wavelength-resolved technology.

The click reaction is a more effective method for DNA ligation compared with the traditional Watson−Crick complementary owing to the higher thermal stability as well as needless of complex base encoding,[29−32] which thus provides

Received: October 22, 2018
Accepted: January 23, 2019
Published: January 23, 2019

DOI: 10.1021/acs.analchem.8b04831
Anal. Chem. 2019, 91, 2861−2868

Scheme 1. Schematic Diagrams of Sensitive PEC Biosensor for the Multiplex Assay[a]

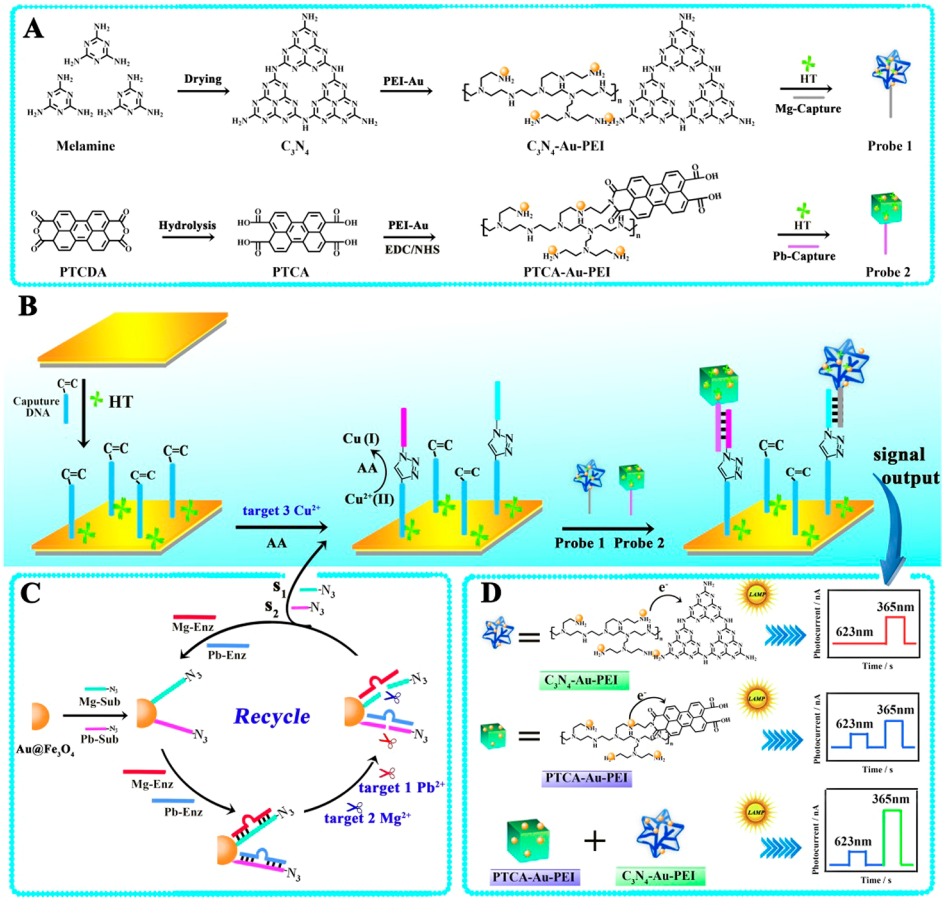

[a](A) Signal probes assembled by wavelength-resolved photoactive materials of PTCA-PEI-Au and C_3N_4-Au-PEI, respectively; (B) fabrication of the PEC biosensor; (C) target-induced cycle output S_1 and S_2 based on ion-dependent DNAzymes co-immobilized $Au@Fe_3O_4$ nanoparticles; and (D) mechanism of photocurrent generation.

the promise for increasing the utilization rate of output DNAs. Hence, in this work, by combining the DNAzymes-assisted cleavage recycling amplification with Cu^{2+} and the ascorbic acid (AA) cocatalyzed click reaction, a novel dual-signal output PEC biosensor using wavelength-resolved technology was designed for efficient and sensitive triplex metal ions detection (Scheme 1). First, the ion-dependent DNAzymes (Pb-Enzy and Mg-Enzy) immobilized on $Au@Fe_3O_4$ could be specially cleaved by Pb^{2+} (target 1) and Mg^{2+} (target 2) to correspondingly release amounts of cycle output DNA fragments, azido-S_1 and azido-S_2, by using DNAzymes-assisted cleavage recycling amplification, which subsequently could be grafted efficiently on the same capture DNA modified electrode via click reaction for further immobilization of two photoactive nanomaterials (synthesized by 3,4,9,10-perylene tetracarboxylic acid, PTCA, and carbon nitride, C_3N_4) labeled with single DNA, respectively, significantly increasing the utilization rate of output DNAs. Thereafter, an obvious distinguishing dual-signal output at 365 and 623 nm could thus be acquired for simultaneously sensitive detection of Pb^{2+} and Mg^{2+} with the use of wavelength-resolved technology. Furthermore, the control variable method was used to sensitively detect Cu^{2+} through altering the concentration of Cu^{2+} in click reaction with improved detection efficiency. The proposed approach not only ingeniously converted the targets into substantial output DNA fragments for photoactive nanomaterials immobilization but also innovatively realized the effective immobilization of diverse cycle output DNAs on the same capture DNA modified electrode through using the click reaction, thereby significantly improving the detection sensitivity. In summary, the click reaction was ingeniously adopted to achieve sensitive detection while greatly improving detection efficiency. Moreover, this click reaction-assist strategy can be extended easily by assembly of various azido-DNA or alkynyl-DNA fragments related to targets such as metal ions, small molecules, and tumor markers, giving impetus to the design of new multiplex PEC approaches with ultimate applications in environmental monitoring, food supervision, and disease diagnosis.

EXPERIMENTAL SECTION

Materials and Reagents. Perylene-3,4,9,10-tetracarboxylic dianhydride (PTCDA) and melamine were purchased from LianGang Dyestuff Chemicals Co. Ltd. (Liaoning, China). Magnesium chloride hexahydrate ($MgCl_2{\cdot}6H_2O$), copper sulfate pentahydrate ($CuSO_4{\cdot}5H_2O$), ascorbic acid (AA), ethanol, and potassium chloride were provided by Kelon Co. Ltd. (Chengdu, China). Lead nitrate ($Pb(NO_3)_2$) was obtained by Guangfu Biaowu Co. Ltd. (Tianjin, China). L-Cysteine (L-Cys) was purchased from J&K Chemical Co. Ltd. (Beijing, China). Amino-modified magnetic microspheres (NH_2-Fe_3O_4, w/v = 0.5%, 10 mL) was provided by BaseLine

DOI: 10.1021/acs.analchem.8b04831
Anal. Chem. 2019, 91, 2861−2868

Table 1. Information of Oligonucleotide Sequences in This Experiment

name	sequence
Pb-Subs	5′-SH-$(CH_2)_6$-GCATACTCACTArAGGAAGAGATG-N_3-3′
Pb-Enzy	5′-CATCTTCTCCGAGCCGGTCGAAATAGTGTATGC-3′
Mg-Subs	5′-SH-$(CH_2)_6$-AATCTGCAGAGTATrAGGATATCC-N_3-3′
Mg-Enzy	5′-GGATATCAGCGATCACCCATGTTACTCTGCAGATT-3′
Capture DNA	5′-SH-$(CH_2)_6$-GACGGGAAGC-C≡CH-3′
Pb-Capture	5′-CATCTCTTCC-NH_2-$(CH_2)_6$-3′
Mg-Capture	5′-GGATACC-NH_2-$(CH_2)_6$-3′

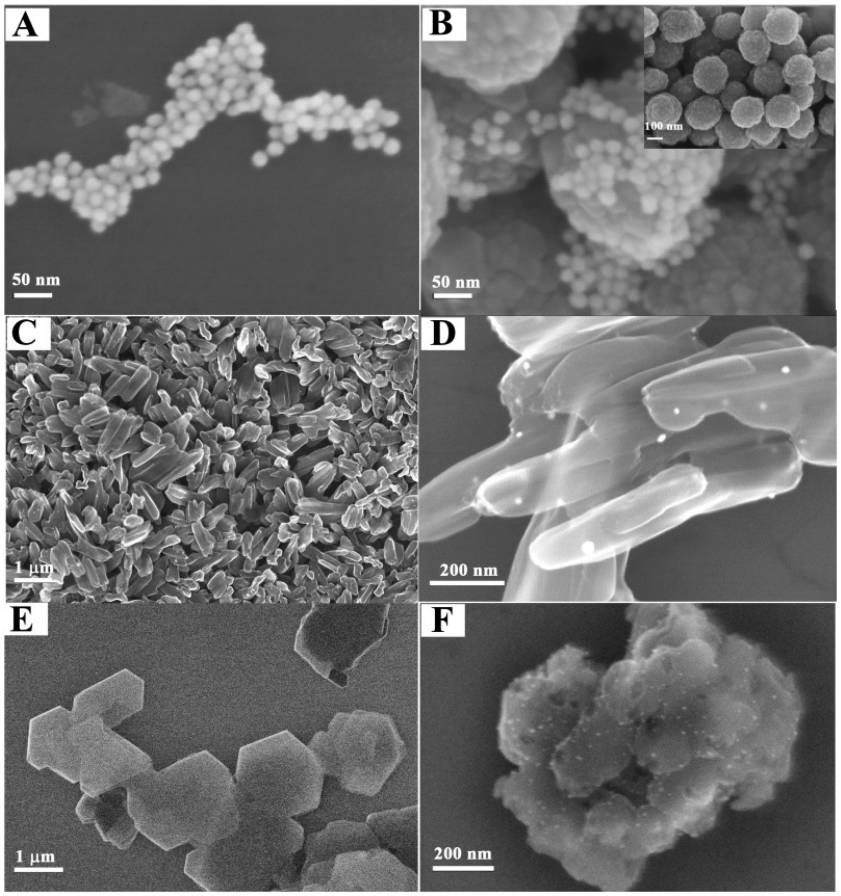

Figure 1. SEM images of (A) PEI-Au nanoparticles, (B) Au@Fe_3O_4 (insert, pure NH_2-Fe_3O_4), (C) PTCA, (D) PTCA-PEI-Au, (E) C_3N_4, and (F) C_3N_4-Au-PEI.

ChromTech Research Centre (Tianjin, China). Gold chloride ($HAuCl_4$), hexanethiol (HT), and polyethylenimine (PEI, average Mn 10 000 by gel permeation chromatography, purity 499%) were purchased from Sigma Co. Ltd. (St. Louis, MO). Phosphate buffered solution (PBS, pH 7.0, 0.1 M) was prepared by 0.1 M Na_2HPO_4, 0.1 M KH_2PO_4, and 0.1 M KCl. Tris-HCl buffer was prepared by 20 mM Tris-HCl, 140 mM NaCl, 5 mM KCl, and 1 mM $CaCl_2$. All oligonucleotides used in this experiment were bought from Sangon Biotech Co. Ltd. (Shanghai, China), and their base sequences were listed in Table 1.

Apparatus. The PEC measurement was performed on a PEC workstation (Ivium, The Netherlands). The excitation light source at 365 and 623 nm was supplied by the LED lamp and switched off-on-off for 10−20−10 s under a 0.0 V potential. Electrochemical deposition of AuNPs (depAu) was conducted in 1% w/v $HAuCl_4$ aqueous solution under −0.2 V for 30 s. Cyclic voltammetry (CV) measurement was operated at a CHI 660e electrochemical workstation (Shanghai Chenhua Instrument, China). $[Fe(CN)_6]^{3-/4-}$ solution (5.0 mM, pH 7.0) was used to measure CV under −0.2 and 0.6 V at a scan rate of 100 mV/s. The morphologies of the nanomaterials were characterized by the scanning electron microscopy (SEM, S-4800, Hitachi, Japan). X-ray photoelectron spectroscopy (XPS) was performed through the VG Scientific ESCALAB 250 spectrometer.

Synthesis of DNAzymes Coimmobilized Au@Fe_3O_4 Nanoparticles. 1 mL 50 mg/L NH_2-Fe_3O_4 was first subjected to 15 mLAuNPs[33] for 12 h reaction at 4 °C to form Au@Fe_3O_4 nanoparticles, which subsequently was followed by the magnetic separation for removing residual AuNPs. Then, the obtained Au@Fe_3O_4 nanoparticles were dispersed in 6 mL of PBS for further use. After that, 200 μL obtained Au@Fe_3O_4 solution was mixed with 10 μL ion-dependent substrate (Pb-Subs and Mg-Subs, 50 μM, respectively) and reacted half of 1 day at 4 °C. Afterward,

DOI: 10.1021/acs.analchem.8b04831
Anal. Chem. 2019, 91, 2861−2868

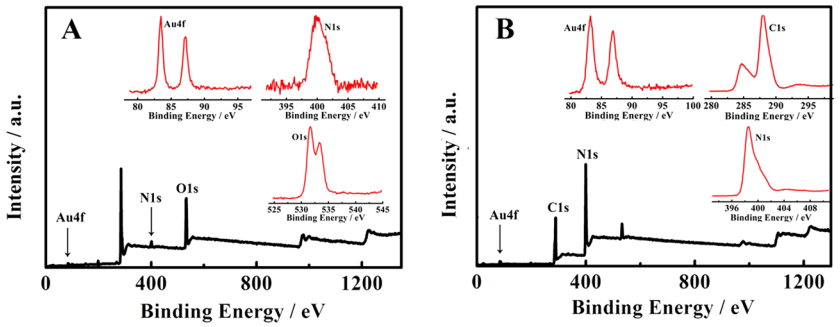

Figure 2. XPS analysis for the full region of (A) PTCA-PEI-Au and (B) C_3N_4-Au-PEI (the insets were XPS analysis for O 1s, C 1s, Au 4f, N 1s, respectively).

10 μL Enzy (Pb-Enzy and Mg-Enzy, 50 μM, respectively) was added to the mixture for 2 h reaction at 25 °C. Since the Pb-Subs and Mg-Subs were hybridized with Pb-Enzy and Mg-Enzy, respectively, the ion-dependent DNAzyme co-immobilized Au@Fe_3O_4 could be formed through hybridization reaction.

Synthesis of Different Detection Probes. Amine-rich polyethylenimine (PEI), as a reductant and linkage platform, was employed to form PEI-Au for the further synthesis of functionalized Au-PEI-conjugated (PTCA-PEI-Au) nanomaterials and PEI-Au-conjugated (C_3N_4-Au-PEI) nanomaterials. To preparation of probe 1 and probe 2, 100 μL 2.5 mM PTCA, which was prepared by hydrolysis of PTCDA in alkaline conditions,[34] was first added into 15 μL 200 mM EDC and 50 mM NHS for stirring 1 h to activate its carboxyl group. After that, 20 μL synthesized PEI-Au[35] was added into the above mixture for 12 h stir to form PTCA-PEI-Au. Then 125 μL prepared PTCA-PEI-Au was mixed with 10 μL 50 μM Pb-Capture and stirred 12 h at 4 °C to successfully obtain probe 2. Meanwhile, 2 mL polymerized C_3N_4[36] was added to 200 μL PEI-Au and stirred 12 h to form C_3N_4-Au-PEI through the amide bond, which followed by adding 10 μL 50 μM Mg-Subs into solution with reaction of 12 h at 4 °C to form probe 1.

Fabrication of the PEC Biosensor for Multiple Assays. The fabricated procedure of the PEC biosensor was illustrated in Scheme 1. Pretreated mirrorlike GCE[37] was immersed in 1% $HAuCl_4$ aqueous solution for electrodeposition of the AuNPs layer. Afterward, 10 μL4 μM Capture DNA was introduced on the electrode and incubated for 12 h at 25 °C, followed by addition of 2 μL HT (1 mM) to block the binding sites. After that, cleavage fragments S_1 and S_2 were dropped on the fabricated electrode, accompanied with the addition of 5 μL Cu^{2+} and AA at a concentration of 1:5 to induce the click reaction under 2 h, 25 °C. Finally, 10 μL 2 μM prepared probe 1 and probe 2 were incubated 2 h at 25 °C to be captured on the electrode via the DNA hybridization of S_1 and S_2.

Principle for Triplex Detection. The fabricated biosensor was rinsed in PBS buffer (0.005 M L-Cys, 0.1 M PBS, pH 7.0) and measured on a PEC workstation. Here, the incubation of Mg^{2+} could lead to the assembly of C_3N_4 functionalized probe 1 on the electrode under the conditions of a sufficient Cu^{2+}-catalyzed click reaction, thereby outputting a negligible photocurrent signal at 623 nm and a significant photocurrent signal at 365 nm. The incubation of Pb^{2+} could immobilize PTCA functionalized probe 2 with a significant photocurrent signal at wavelengths of 623 and 365 nm. Ingeniously, owing to no energy transfer between the two wavelength-selective photoactive nanomaterials, the generated signals do not interfere with each other. Therefore, quantification of Pb^{2+} was made only through photocurrent signal at a wavelength of 623 nm. The quantification of Mg^{2+} was performed by eliminating the photocurrent signal generated in the presence of Pb^{2+} at 365 nm. This principle indicated that the fabricated biosensor can be employed to simultaneously detect Pb^{2+} and Mg^{2+} under the conditions of adding sufficient dosage of Cu^{2+} for the complete click reaction. Furthermore, with the addition of enough Pb^{2+} and Mg^{2+}, the assay of Cu^{2+} was carried out at a wavelength of 365 nm. In conclusion, the detection of the three ions was carried out through taking full advantage of the two-step method and distinguishing the dual-signal output strategy.

RESULTS AND DISCUSSION

Morphology Characterization of the Synthetic Materials. The morphology and size of nanomaterials were investigated by SEM. As indicted in Figure 1A, owing to the strong interaction between Au nanoparticles and dendritic polymer PEI, PEI-Au nanoparticles displayed a dendritic structure with an abundance of spherical Au nanoparticles together. After its assembly on the NH_2-Fe_3O_4 surface, uniformly globular PEI-Au with a diameter of 200 nm can be seen on the surface of NH_2-Fe_3O_4 (Figure 1B). The insert in Figure 1B was the SEM of pure NH_2-Fe_3O_4. Moreover, as illustrated in Figure 1C, the obtained PTCA presented stick shapes with a width of 300 nm. When PTCA was linked with PEI-Au, it can be clearly seen that generous bright dots were adhered on PTCA (Figure 1D), implying the successful preparation of PTCA-PEI-Au. Figure 1E was the SEM of synthesized C_3N_4, which exhibited a sheetlike structure approximately to 500 nm in diameter. After its decoration with PEI-Au to form C_3N_4-Au-PEI, amounts of bright dots can also be seen (Figure 1F).

Additionally, the elemental analysis performed by XPS was also used to further characterize the ingredient of different materials. As shown in Figure 2A, XPS peaks at 83 eV, 400 eV, and 532 eV were, respectively, assigned to Au 4f, N 1s, and O 1s, which correspondingly indicted the composition of Au, PEI and PTCA in synthetic PTCA-PEI-Au. Similarly, the spectra of Au 4f, N 1s, and C 1s assigned to 83 eV, 400 eV, and 285 eV, respectively, proved the successful preparation of C_3N_4-Au-PEI (Figure 2B).

Electrochemical and PEC Characterizations of the Biosensor. CV measurements performed in 5.0 mM $[Fe(CN)_6]^{3-/4-}$ solution was utilized to characterize assembly processes of the working electrode step-by-step. Corresponding CV curves were shown in Figure 3A. In compared with

DOI: 10.1021/acs.analchem.8b04831
Anal. Chem. 2019, 91, 2861−2868

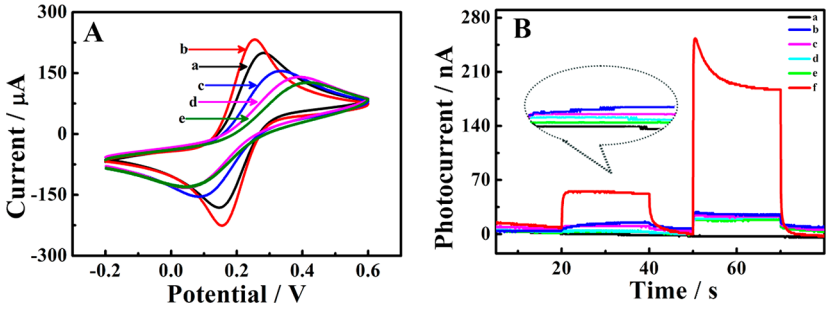

Figure 3. (A) CV profiles of (a) bare GCE, (b) depAu/GCE, (c) capture DNA/depAu/GCE, (d) HT/capture DNA/depAu/GCE, and (e) S_1, S_2/HT/capture DNA/depAu/GCE. The CV measurements were performed in 5.0 mM $[Fe(CN)_6]^{3-/4-}$ solution. (B) The PEC profiles of (a) bare GCE, (b) depAu/GCE, (c) capture DNA/depAu/GCE, (d) HT/capture DNA/depAu/GCE, (e) S_1, S_2/HT/capture DNA/depAu/GCE, and (f) S_1, S_2/HT/capture DNA/depAu/GCE after assembly of probe 1, probe 2. The PEC measurements were detected in 4 mL of 0.1 M PBS (pH 7.0) containing 0.005 M L-Cys.

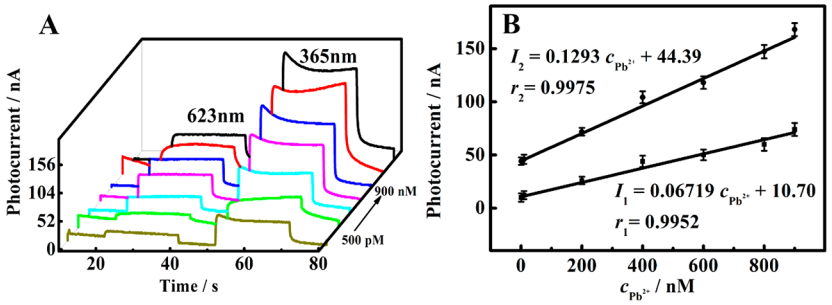

Figure 4. (A) Photocurrent response of the biosensor with different concentrations of Pb^{2+}: 500 pM, 10 nM, 200 nM, 400 nM, 600 nM, 800 nM, 900 nM and (B) corresponding linear calibration curve at the wavelength of 623 and 365 nm.

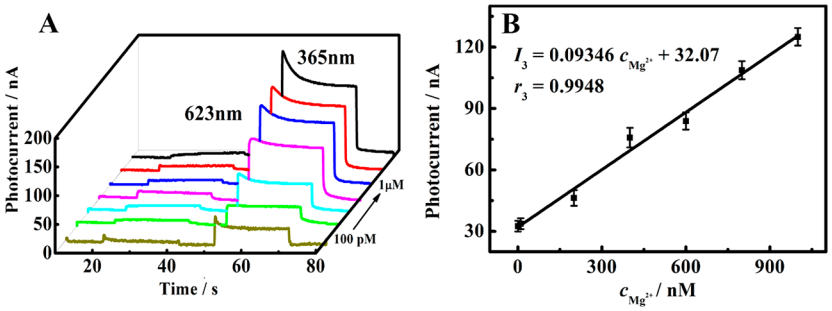

Figure 5. (A) Photocurrent response of the biosensor with different concentrations of Mg^{2+}: 100 pM, 10 nM, 200 nM, 400 nM, 600 nM, 800 nM, 1 μM and (B) corresponding linear calibration curve at the wavelength of 365 nm.

bare GCE (curve a), the peak current of conductive depAu coated GCE increased owing to the excellent conductivity of depAu (curve b). However, after introducing the negatively charged capture DNA on depAu/GCE, the peak current slightly decreased by reason for the electronic repulsion between $[Fe(CN)_6]^{3-/4-}$ and capture DNA (curve c). Once the HT was employed to block nonspecific binding sites of the electrode, a further decreased peak current was appeared in virtue of hindrance of electron transfer (curve d). There was a further reduced peak current after the HT/capture DNA/depAu/GCE was immobilized with produced DNA S_1 and S_2 via click reaction (curve e).

Furthermore, PEC characterization was also carried out to investigate the assembly processes (Figure 3B), which performed in 4 mL of 0.1 M PBS (pH 7.0) containing 0.005 M L-Cys. As we know, the photoactive material is a key factor for producing photocurrent signal. Therefore, owing to absence of photoactive material, there were negligible photocurrent signals for the (a) bare GCE, (b) depAu/GCE, (c) capture DNA/depAu/GCE, (d) HT/capture DNA/depAu/GCE, and (e) S_1, S_2/HT/capture DNA/depAu/GCE. However, with the superior conductivity of depAu, the background signal of depAu/GCE was higher compared to that of bare GCE. Additionally, owing to the inert property of DNA and HT, the background signal of capture DNA/depAu/GCE, HT/capture DNA/depAu/GCE, and S_1, S_2/HT/capture DNA/depAu/GCE successively reduced compared with that of depAu/GCE. Finally, the immobilization of probe 1 and probe 2 containing the photoactive materials of C_3N_4-Au-PEI and PTCA-PEI-Au, respectively, caused a remarkable increase of photocurrent at wavelengths of 623 and 365 nm (curve f).

Analytical Performance and Feasibility Analysis. The performance of PEC biosensors was evaluated via quantitative detection of Pb^{2+}, Mg^{2+} and Cu^{2+}. Signal outputs increased linearly with the increase concentrations of Pb^{2+} (500 pM, 10 nM, 200 nM, 400 nM, 600 nM, 800 nM, 900 nM) at

DOI: 10.1021/acs.analchem.8b04831
Anal. Chem. 2019, 91, 2861−2868

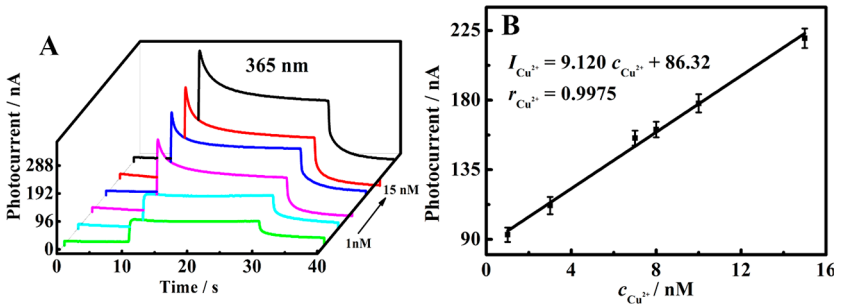

Figure 6. (A) Photocurrent response of the biosensor with different concentrations of Cu^{2+}: 1 nM, 3 nM, 7 nM, 8 nM, 10 nM, 15 nM and (B) corresponding linear calibration curve at a wavelength of 365 nm.

Table 2. Comparison between Theoretical Value and Actual Value

	actual added amounts/nM		detection amounts/nM		ratio/% (found/added)		RSD/%	
sample number	Mg^{2+}	Pb^{2+}	Mg^{2+}	Pb^{2+}	Mg^{2+}	Pb^{2+}	Mg^{2+}	Pb^{2+}
1	0.1	0.5	0.0811	0.5921	81.10	118.42	5.4	3.8
2	10	10	10.194	10.1214	119.4	112.14	3.2	2.7
3	200	200	209.18	189.84	104.59	94.92	5.8	3.5
4	400	400	483.13	491.03	96.63	98.20	4.1	3.1
5	600	600	602.56	585.55	100.43	97.59	2.9	4.2
6	800	800	789.90	843.48	98.74	105.4	4.9	3.7
7	1000	900	100.743	925.31	100.743	102.81	2.7	3.9

Table 3. Comparison of Various Multiplex Detection Methods of Heavy Metal Ions

detection method	detection range	detection limit	ref
electrochemical	Ag^{+} (10−150 nM) Hg^{2+} (10−100 nM)	Ag^{+} (3.4 nM) Hg^{2+} (1.7 nM)	38
fluorescence	Zn^{2+} (1−30 nM) Cu^{2+} (1−20 nM)	Zn^{2+} (0.47 nM) Cu^{2+} (0.45 nM)	39
fluorescence	Ag^{+} (6−650 nM) Hg^{2+} (5−1 μM)	Ag^{+} (1.2 nM) Hg^{2+} (3.3 nM)	40
fluorescence	Zn^{2+} (0.25−2 nM) Cu^{2+} (0.1−5 nM)	Zn^{2+} (0.1 nM) Cu^{2+} (0.08 nM)	41
electrochemiluminescence	Ni^{2+} (0−120 nM) Cd^{2+} (0.1−4 μM)	Ni^{2+} (1 nm) Cd^{2+} (20 nM)	42
surface-enhanced Raman scattering	Ag^{+} (0.1−10 μM) Hg^{2+} (1−10 μM)	Ag^{+} (0.86 nM) Hg^{2+} (0.77 nM)	43
PEC	Pb^{2+} (500 pM−900 nM) Mg^{2+} (100 pM−1 μM)	Pb^{2+} (166 pM) Mg^{2+} (34 pM)	our work

wavelengths of 623 and 365 nm (Figure 4A). As shown in Figure 4B, the corresponding linear regression equation are $I_1 = 0.06719c_{Pb}{}^{2+} + 10.70$ (I_1 represent photocurrent intensity of detecting Pb^{2+} at 623 nm, $c_{Pb}{}^{2+}$ represented the concentration of Pb^{2+}) and $I_2 = 0.1293c_{Pb}{}^{2+} + 44.39$ (I_2 represent photocurrent intensity of detecting Pb^{2+} at 365 nm). However, there was a negligible photocurrent signal at 623 nm and obvious changes at 365 nm (Figure 5A) with different concentrations of Mg^{2+} (100 pM, 10 nM, 200 nM, 400 nM, 600 nM, 800 nM, 1 μM), Figure 5B showed a linear relationship between photocurrent intensity and concentration in the range of 100 pM to 1 μM, the corresponding linear equation at wavelengths of 365 nm was $I_3 = 0.09346c_{Mg}{}^{2+} + 32.07$ (I_3 represented the photocurrent signal of detecting Mg^{2+} at 365 nm, $c_{Mg}{}^{2+}$ represented the concentration of Mg^{2+}), and the added error bar at all the figures implied the detection standard deviation ($n = 8$).

Since photoactive nanomaterials generated signals did not interfere with each other, Pb^{2+} was quantified only through photocurrent signal at a wavelength of 623 nm. The quantification of Mg^{2+} was performed by eliminating the photocurrent signal generated in the presence Pb^{2+} of at 365 nm. Therefore, a final linear equation of concentration and photocurrent intensity could be simulated, and the corresponding linear regression equation is shown in eqs 1 and 2, respectively.

$$I_{Pb^{2+}} = 0.06719c_{Pb^{2+}} + 10.70 \quad (1)$$

$$I_{Mg^{2+}} = 0.1293c_{Pb^{2+}} + 0.093346c_{Mg^{2+}} + 76.46 \quad (2)$$

where $I_{Pb}{}^{2+}$ and $I_{Mg}{}^{2+}$ represented photocurrent intensity of detecting Pb^{2+} and Mg^{2+} at 623 and 365 nm, respectively, and the estimated detection limits (defined as LOD = $3S_b/m$, where S_b is the standard deviation of the blank signals, and m is the analytical sensitivity, which can be estimated as the slope of calibration curve at lower concentration ranges) are 166 pM and 34 pM, respectively.

DOI: 10.1021/acs.analchem.8b04831
Anal. Chem. 2019, 91, 2861−2868

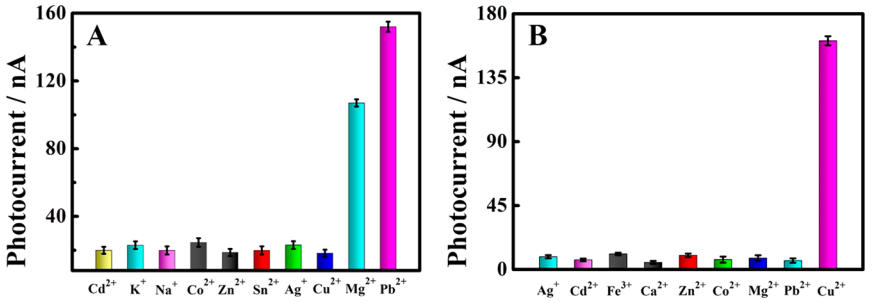

Figure 7. Selectivity of the fabricated biosensor (A) for the detection of Mg^{2+} and Pb^{2+} in comparison with the 10-fold (8 μM) excess of other ions including Cd^{2+}, K^+, Na^+, Co^{2+}, Zn^{2+}, Sn^{2+}, Cu^{2+} and Ag^+ and (B) for the detection of Cu^{2+} against with 10-fold (15 nM) different nontargets containing Ag^+, Cd^{2+}, Fe^{3+}, Ca^{2+}, Zn^{2+} Co^{2+}, Mg^{2+} and Pb^{2+}.

Furthermore, this PEC biosensor also can be used for the detection of Cu^{2+}. The output signals at 365 nm, which is shown in Figure 6A, increased linearly with a concentration of Cu^{2+}. As presented in Figure 6B, the corresponding linear equation was $I_{Cu}{}^{2+} = 9.120c_{Cu}{}^{2+} + 86.32$ ($I_{Cu}{}^{2+}$ indicated the photocurrent intensity of detecting Cu^{2+} at 365 nm, $c_{Cu}{}^{2+}$ is the concentration of Cu^{2+}) in the range of 1 nm to 15 nM, and the detection limit (defined as LOD = $3S_b/m$, where S_b is the standard deviation of the blank signals, and m is the analytical sensitivity which can be estimated as the slope of the calibration curve at lower concentration ranges) was 0.33 nM.

To prove that the simulated linear equation could be applied for simultaneous complex detection in the practical sample, different amount of Pb^{2+} (500 pM, 10 nM, 200 nM, 400 nM, 600 nM, 800 nM, 900 nM) and Mg^{2+} (100 pM, 10 nM, 200 nM, 400 nM, 600 nM, 800 nM, 1 μM) were simultaneously added into water, followed by detection with a fabricated PEC biosensor. Figure S2 shows the PEC signal output of the practical sample detection, and Table 2 indicates the comparison of actual added concentrations and detection concentrations. It was found that there is no significant deviation between the actual added amounts and theoretical amounts, which demonstrates that the established simultaneous detection PEC biosensor could be employed as a metal ion assay. In addition, the comparison of recent multiplex detection methods of metal ions was made with our method. As shown in Table 3, owing to the combination of the click reaction and the ion-induced cleavage recycling amplification strategy, the fabricated PEC biosensor is more sensitive and has a lower detection limit than some recent multiplex metal ion assays.

Selectivity of the Proposed PEC Biosensor. The selectivity of the fabricated biosensor for the detection of Mg^{2+} and Pb^{2+} was evaluated in comparison with 10-fold (8 μM) excess of other interference ions including Cd^{2+}, Na^+, K^+, Cd^{2+}, Co^{2+}, Zn^{2+}, Sn^{2+}, Cu^{2+} and Ag^+. As shown in Figure 7A, no significant signal changes were observed despite the high concentration of the interfering metal ions, and the added error bar implied the detection standard deviation (n = 8). However, in the presence of Mg^{2+} or Pb^{2+}, even at a much lower concentration, the photocurrent signal at a wavelength of 365 nm sharply increased, illustrating that the proposed biosensor had good selectivity to detect target metal ions. Furthermore, the selectivity of the fabricated biosensor for the detection of Cu^{2+} was investigated. As shown in Figure 7B, even the addition of 10-fold interference ions, such as Ag^+, Cd^{2+}, Fe^{3+}, Ca^{2+}, Zn^{2+} Co^{2+}, $Mg^{2+}$and Pb^{2+}, the photocurrent signals were extremely tiny in comparison with the concentration as low as 15 nM Cu^{2+}.

CONCLUSION

In summary, we have fabricated a dual-signal output PEC strategy for sensitive triplex metal ions detection by combining the click reaction with cleavage recycling amplification. Here, the cleavage cycle output DNAs used for assembling diverse photoactive nanomaterials was first ligated on the same capture DNA modified electrode via click reaction with significantly increased utilization rate of cycle output DNAs, which not only realized simultaneously sensitive detection of Pb^{2+} and Mg^{2+} with wavelength-resolved technology but also achieved a Cu^{2+} assay via the control variable method. Moreover, this proposed strategy provided a new PEC multiple sensitive detection model, holding a great potential application in environmental monitoring, food supervision, and disease diagnosis.

ASSOCIATED CONTENT

Supporting Information

The Supporting Information is available free of charge on the ACS Publications website at DOI: 10.1021/acs.analchem.8b04831.

Measurement conditions optimization of the fabricated biosensor and application of proposed PEC biosensor for simultaneous complex detection in the practical sample (PDF)

AUTHOR INFORMATION

Corresponding Authors

*Phone: +86-23-68252277. Fax: +86-23-68253172. E-mail: yuanruo@swu.edu.cn.

*E-mail: y198688@swu.edu.cn.

ORCID

Ya-Qin Chai: 0000-0003-4392-9592

Ruo Yuan: 0000-0003-3664-6236

Notes

The authors declare no competing financial interest.

ACKNOWLEDGMENTS

This work was supported by the National Natural Science Foundation (NNSF) of China (Grants 21505107, 51473136, and 21575116), the Chongqing Research Program of Basic Research and Frontier Technology (Grant cstc2018jcyjA0797), and the Fundamental Research Funds for the Central Universities (Grant SWU117045).

DOI: 10.1021/acs.analchem.8b04831
Anal. Chem. 2019, 91, 2861−2868

REFERENCES

(1) Zhao, W. W.; Xu, J. J.; Chen, H. Y. *Chem. Rev.* **2014**, *114*, 7421−7441.
(2) Tu, W. W.; Cao, H. J.; Zhang, L.; Bao, J. C.; Liu, X. H.; Dai, Z. H. *Anal. Chem.* **2016**, *88*, 10459−10465.
(3) Zhao, W. W.; Xu, J. J.; Chen, H. Y. *Anal. Chem.* **2018**, *90*, 615−627.
(4) Yu, L. M.; Zhu, Y. C.; Liu, Y. L.; Qu, P.; Xu, M. T.; Shen, Q.; Zhao, W. W. *Anal. Chem.* **2018**, *90*, 10803−10811.
(5) Li, C. X.; Wang, H. Y.; Shen, J.; Tang, B. *Anal. Chem.* **2015**, *87*, 4283−4291.
(6) Zhao, W. W.; Xu, J. J.; Chen, H. Y. *Chem. Soc. Rev.* **2015**, *44*, 729−741.
(7) Osterloh, F. E. *Chem. Soc. Rev.* **2013**, *42*, 2294−2320.
(8) Hou, T.; Xu, N. N.; Wang, W. X.; Ge, L.; Li, F. *Anal. Chem.* **2018**, *90*, 9591−9597.
(9) Ma, Z. Y.; Pan, J. B.; Lu, C. Y.; Zhao, W. W.; Xu, J. J.; Chen, H. Y. *Chem. Commun.* **2014**, *50*, 12088−12090.
(10) Song, Z.; Fan, G. C.; Li, Z. M.; Gao, F. X.; Luo, X. L. *Anal. Chem.* **2018**, *90*, 10681−10687.
(11) Zhao, W. W.; Ma, Z. Y.; Yu, P. P.; Dong, X. Y.; Xu, J. J.; Chen, H. Y. *Anal. Chem.* **2012**, *84*, 917−923.
(12) Li, J.; Tu, W. W.; Li, H. B.; Han, M.; Lan, Y. Q.; Dai, Z. H.; Bao, J. C. *Anal. Chem.* **2014**, *86*, 1306−1312.
(13) Wang, H.; Zhang, B. H.; Zhao, F. Q.; Zeng, B. Z. *ACS Appl. Mater. Interfaces* **2018**, *10*, 35281−35288.
(14) Zhang, Y. F.; Xu, R.; Kang, Q.; Zhang, Y.; Wei, Q.; Wang, Y. G.; Ju, H. X. *ACS Appl. Mater. Interfaces* **2018**, *10*, 31080−31087.
(15) Wang, Q.; Ruan, Y. F.; Zhao, W. W.; Lin, P.; Xu, J. J.; Chen, H. Y. *Anal. Chem.* **2018**, *90*, 3759−3765.
(16) Zhang, X. R.; Guo, Y. S.; Liu, M. S.; Zhang, S. S. *RSC Adv.* **2013**, *3*, 2846−2857.
(17) Hao, Q.; Shan, X. N.; Lei, J. P.; Zang, Y.; Yang, Q. H.; Ju, H. X. *Chem. Sci.* **2016**, *7*, 774−780.
(18) Wang, J.; Song, M. M.; Hu, C. G.; Wu, K. B. *Anal. Chem.* **2018**, *90*, 9366−9373.
(19) El Harakeh, M.; Alawieh, L.; Saouma, S.; Halaoui, L. I. *Phys. Chem. Chem. Phys.* **2009**, *11*, 5962−5973.
(20) Cai, G. N.; Yu, Z. Z.; Ren, R. R.; Tang, D. P. *ACS Sens* **2018**, *3*, 632−639.
(21) Qileng, A.; Wei, J.; Lu, N.; Liu, W.; Cai, Y.; Chen, M.; Lei, H.; Liu, Y. *Biosens. Bioelectron.* **2018**, *106*, 219−226.
(22) Lv, S.; Zhang, K.; Zeng, Y.; Tang, D. *Anal. Chem.* **2018**, *90*, 7086−7093.
(23) Zhang, K.; Lv, S.; Lin, Z.; Li, M.; Tang, D. *Biosens. Bioelectron.* **2018**, *101*, 159−166.
(24) Wang, J.; Liu, Z. H.; Hu, C. G.; Hu, S. H. *Anal. Chem.* **2015**, *87*, 9368−9375.
(25) Wang, J.; Long, J.; Liu, Z. H.; Wu, W. Z.; Hu, C. G. *Biosens. Bioelectron.* **2017**, *91*, 53−59.
(26) Dai, H.; Zhang, S. P.; Hong, Z. S.; Lin, Y. Y. *Anal. Chem.* **2016**, *88*, 9532−9538.
(27) Zhang, N.; Ma, Z. Y.; Ruan, Y. F.; Zhao, W. W.; Xu, J. J.; Chen, H. Y. *Anal. Chem.* **2016**, *88*, 1990−1994.
(28) Zheng, Y. N.; Liang, W. B.; Yuan, Y. L.; Xiong, C. Y.; Xie, S. B.; Wang, H. J.; Chai, Y. Q.; Yuan, R. *Biosens. Bioelectron.* **2016**, *81*, 423−430.
(29) Gramlich, P. M. E.; Wirges, C. T.; Manetto, A.; Carell, T. *Angew. Chem., Int. Ed.* **2008**, *47*, 8350−8358.
(30) Furst, A.; Landefeld, S.; Hill, M. G.; Barton, J. K. *J. Am. Chem. Soc.* **2013**, *135*, 19099−19102.
(31) Moses, J. E.; Moorhouse, A. D. *Chem. Soc. Rev.* **2007**, *36*, 1249−1262.
(32) Holub, J. M.; Kirshenbaum, K. *Chem. Soc. Rev.* **2010**, *39*, 1325−1337.
(33) Grabar, K. C.; Freeman, R. G.; Hommer, M. B.; Natan, M. *Anal. Chem.* **1995**, *67*, 735−743.
(34) Ma, M. N.; Zhang, X.; Zhuo, Y.; Chai, Y. Q.; Yuan, R. *Nanoscale* **2015**, *7*, 2085−2092.
(35) Jin, L. Y.; Gao, X.; Wang, L. S.; Wu, Q.; Chen, Z. C.; Lin, X. F. J. *Electroanal. Chem.* **2013**, *692*, 1−8.
(36) Yu, H. J.; Shang, L.; Bian, T.; Shi, R.; Waterhouse, G. I. N.; Zhao, Y. F.; Zhou, C.; Wu, L. Z.; Tung, C. H.; Zhang, T. R. *Adv. Mater.* **2016**, *28*, 5080−5086.
(37) Zhang, Y. W.; Liu, J. H.; Wu, G.; Chen, W. *Nanoscale* **2012**, *4*, 5300−5303.
(38) Miao, P.; Tang, Y. G.; Wang, L. *ACS Appl. Mater. Interfaces* **2017**, *9*, 3940−3947.
(39) Li, L.; Feng, J.; Fan, Y. Y.; Tang, B. *Anal. Chem.* **2015**, *87*, 4829−4835.
(40) Zuo, X. W.; Zhang, H. G.; Zhu, Q.; Wang, W. F.; Feng, J.; Chen, X. G. *Biosens. Bioelectron.* **2016**, *85*, 464−470.
(41) Si, H. B.; Sheng, R. J.; Li, Q. L.; Feng, J.; Li, L.; Tang, B. *Anal. Chem.* **2018**, *90*, 8785−8792.
(42) Zhou, Z. X.; Shang, Q. W.; Shen, Y. F.; Zhang, L. Q.; Zhang, Y. Y.; Lv, Y. Q.; Li, Y.; Liu, S. Q.; Zhang, Y. J. *Anal. Chem.* **2016**, *88*, 6004−6010.
(43) Zeng, Y.; Ren, J. Q.; Shen, A. G.; Hu, J. M. *ACS Appl. Mater. Interfaces* **2016**, *8*, 27772−27778.

DOI: 10.1021/acs.analchem.8b04831
Anal. Chem. 2019, 91, 2861−2868